Supplementary Information

Magnetoelectric coupling effects on band alignments of the multiferroic In$_2$Se$_3$-CrI$_3$ trilayer heterostructures

Xueying Liu, [a, †] Chenhai Shen,[a, †] Xueping Li,[a,b] Tianxing Wang,[a] Mengjie He,[a] Lin Li,[a] Ying Wang,[a] Jingbo Li*[c] and Congxin Xia*[a]

[a]Department of Physics, Henan Normal University, Xinxiang 453007, China. E-mail: xiacongxin@htu.edu.cn

[b]College of Electronic and Electrical Engineering, Henan Normal University, Xinxiang, Henan, 453007, China

[c]Institute of Semiconductors, South China Normal University, Guangzhou 510631, China. E-mail: jbli@m.scnu.edu.cn

† These authors have contributed equally.
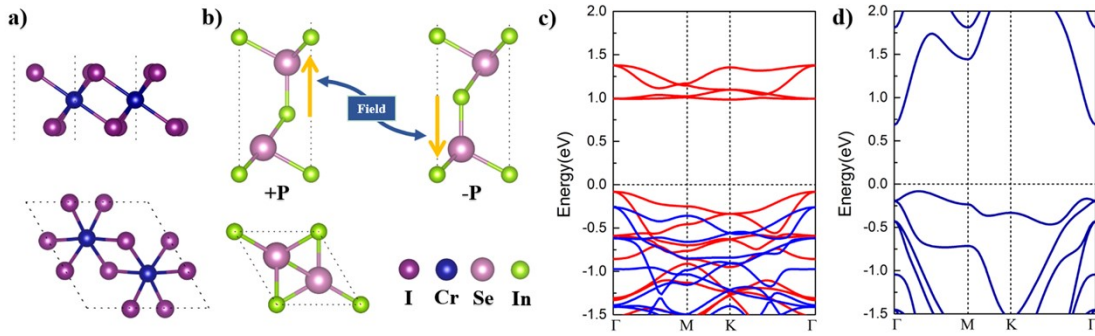
Fig. S1 Side and top view of (a) CrI_3 (b) In_2Se_3 monolayers, where I, Cr, Se, and In atoms are denoted by purple, dark blue, pink, and light green balls, respectively. The diamond-shaped dotted line represents the primitive cell. The band structure of CrI_3 and In_2Se_3 are shown in(c) and (d). The red and blue lines in the Figure (c) represent the energy bands of the spin-up and spin-down channels.
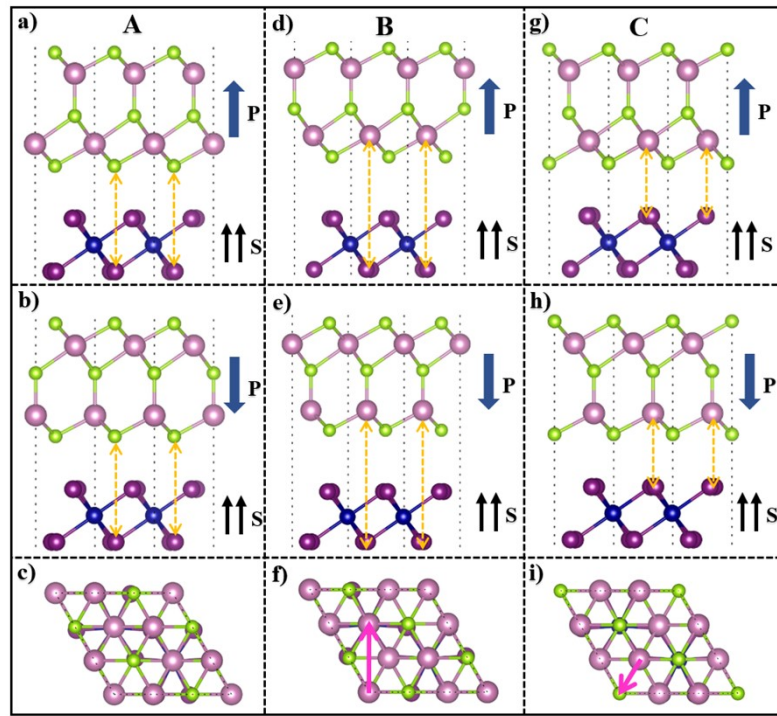
Fig. S2 Side (the upper two panels) and top (bottom panels) view of CrI_3/In_2Se_3 vdWHs in three stackings: A, B and C. Here, the dark blue arrow marked as P indicates the direction of FE polarization, and the black arrow labeled as S represents the spin orientation of Cr atoms. In Fig (f) and (i), the translational displacement of In_2Se_3 relative to CrI_3 are marked by magenta arrows.

For the vertical CrI_3/In_2Se_3 multiferroic vdWHs, we constructed three

typical atomic stackings, i.e. A, B, and C. In view of two polarization states of In_2Se_3, each stacking corresponds to two structures, as shown in Fig. S1. The corresponding stabilities and structural parameters are depicted in Table S2. For A superposition, the lower I atoms are located directly below the bottom Se atoms of In_2Se_3, while the two Cr atoms are located directly below the bottom In atoms of In_2Se_3. We constructed the B and C stacking patterns by shifting the In_2Se_3 of the A stacking along the directions marked by pink arrows.
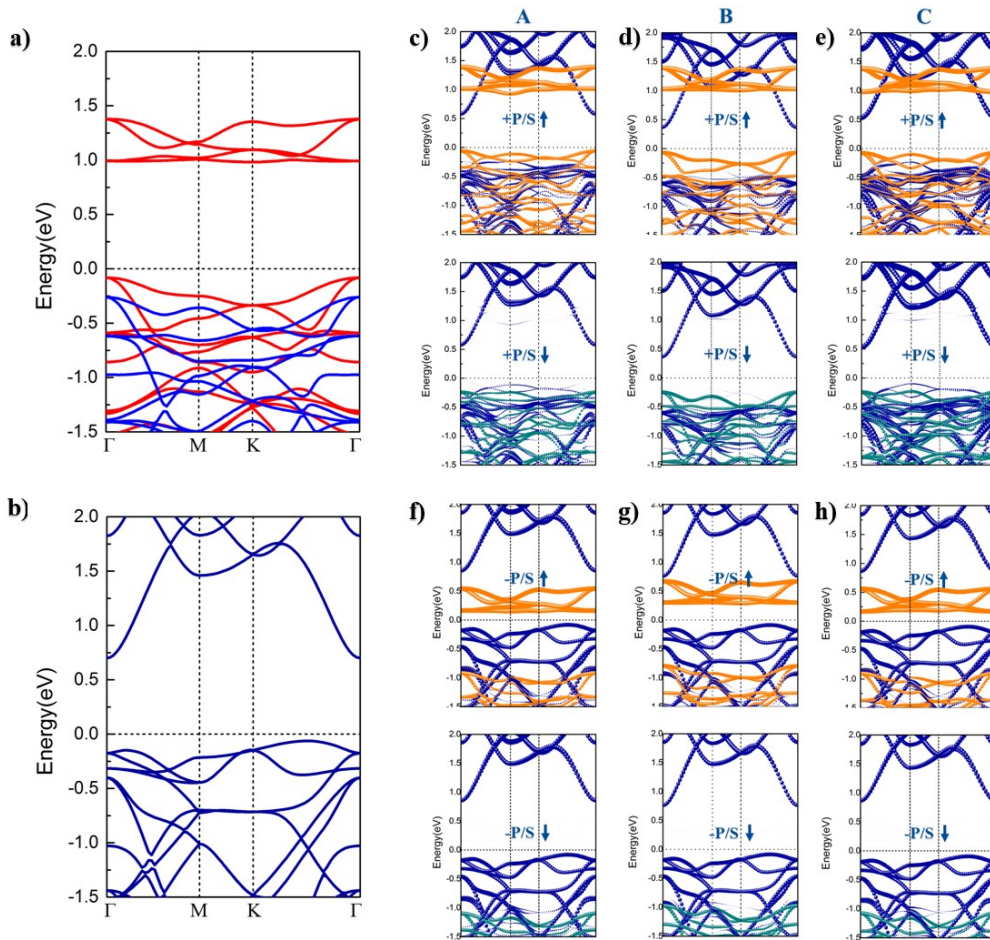

Fig. S3 Spin-polarized band structures of (a) monolayer CrI_3 (b) $\sqrt{3}\times\sqrt{3}$ In_2Se_3. (c-h) CrI_3/In_2Se_3 bilayer vdWHs with A, B and C three stacking patterns. The red and blue lines in Fig. (a) represent the band structures of the spin-up and spin-down channels. In Fig. (c-h), orange and green lines represent the contribution of CrI_3, and dark blue lines represents the contribution of In_2Se_3.

Fig. S3. shows the spin-polarized band structures of above bilayer

vdWHs. Notably, whether combined with +P or −P In_2Se_3, CrI_3 still retains the intrinsic semiconductor. As seen from the Figs. S3(c-e) or S3(f-h), different stacking patterns have little effect on band structures except for a slight shift of the band edges. For +P cases [Fig. S3(c-e)], the band structures of vdWHs can be regarded as a simple superposition of two monolayers. Thus both CrI_3 and In_2Se_3 maintain their intrinsic semiconductor characteristics well. Comparing the Figs. S3(c) and 3(f), it is observed that for the same atoms superposition, the band edge shifts downward when the polarization is reversed to −P case, resulting that the conduction band edge of CrI_3 approach to the fermi level (E_f).

Usually, a smaller interlayer distance within vdWH indicates a stronger vdW interlayer interaction. Table S2 reveals that the A configuration has the strongest interlayer interaction among the three stacking configurations. Moreover, as shown in Fig. S3, the conduction band minimum (CBM) of A stacking with −P polarization is the closest to the Fermi level (E_f). Both the strongest interlayer interaction and the CBM closest to the E_f decide that the A stacking is the most promising to be regulated as a half-metal. Thus, in the following calculations, we conducted some further investigations for the A stacking.

Decreasing the interlayer distance d is a straightforward way to tune the features of 2D materials. The interlayer distance has a very limited influence on the electronic structure of the CrI_3 monolayer inside $CrI_3/(−P)In_2Se_3$ vdWH [Fig. S3]. At this point, we focused on other methods to regulate the magnetoelectric coupling effect, including adding a FE or FM monolayer to the hetero-bilayer structures.
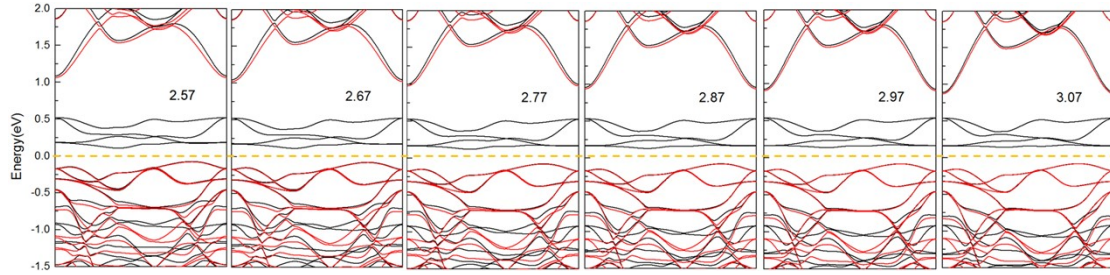
**Fig. S4** The effect of interlayer distance d on the band structures of CrI_3/In_2Se_3 vdWHs for A stacking configuration, ranging from 2.57Å to 3.07Å.
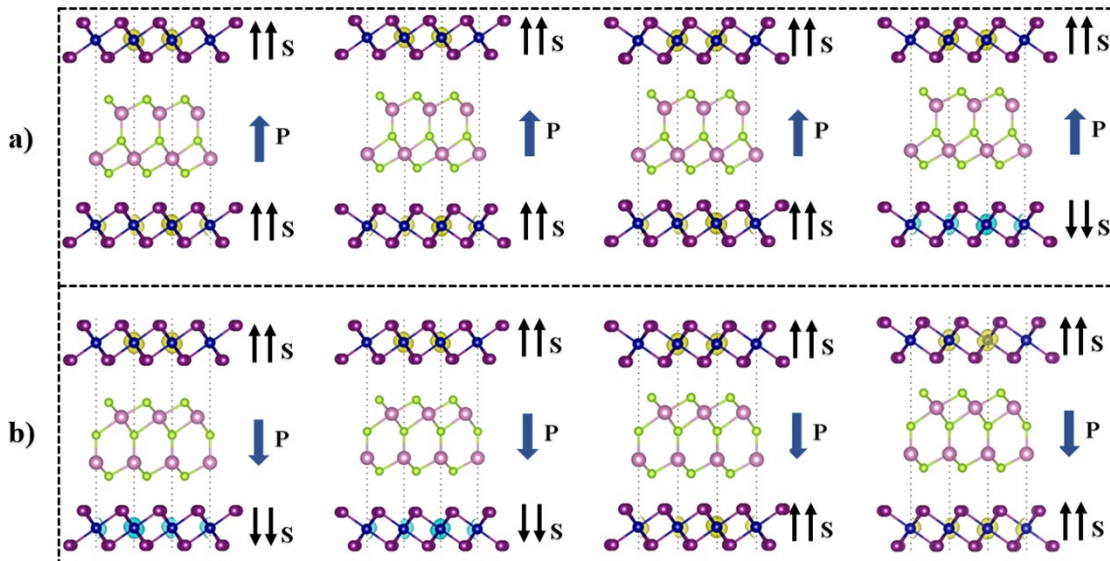
Fig. S5 The structure of $CrI_3/In_2Se_3/CrI_3$ vdWHs with A_1, A_2, A_3 and A_4 stackings for (a) +P and (b) –P case, where the yellow (blue) color around Cr atoms means the spin-up(spin-dw) charge distribution. The black and dark blue arrow arrows indicate the spin orientation of Cr atoms and the direction of ferroelectric polarization.

The A_1 pattern was constructed by inserting In_2Se_3 layer between bilayer CrI_3 layers. As for the A_2 stacking, the lower CrI_3 layer was flipped vertically along the diagonal direction with respect to A_1 stacking. For A_3 superposition, flipping engineering was applied to the upper CrI_3 layer. And for A_4 alignment, both CrI_3 layers were flipped vertically.
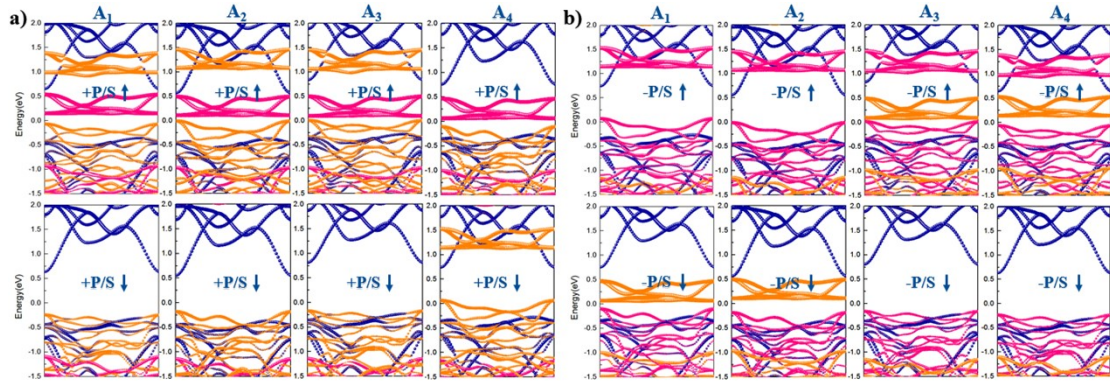
Fig. S6 The spin- and layer-resolved band structures of $CrI_3/In_2Se_3/CrI_3$ vdWHs with (a) +P case (b) –P case, where the A_1, A_2, A_3 and A_4 configurations represent the structures without flipping and applying flipping, respectively. The orange and magenta lines represent the contributions of different CrI_3 layers with the majority spin (S↑) and minority spin (S↓) channels, while dark blue lines denote the contributions of In_2Se_3.
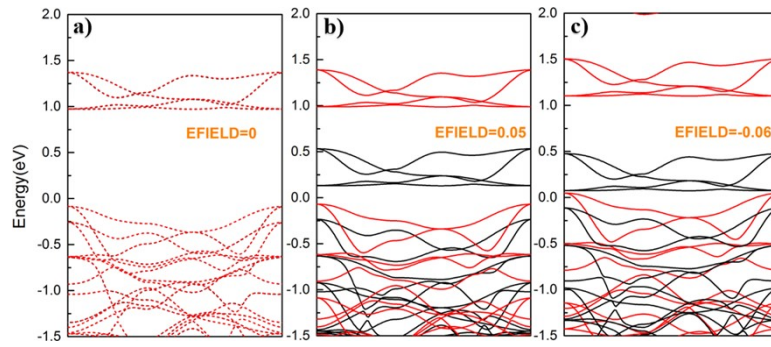
Fig. S7 The band structures of bilayer CrI_3 under certain E-fields (a) 0eV/Å, (b) 0.05eV/Å, (c) -0.06eV/Å.
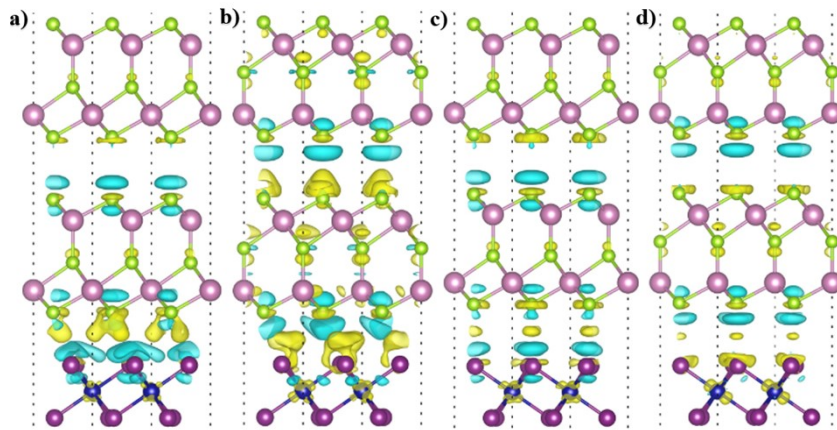
Fig. S8 Differential charge density of $CrI_3/2L-In_2Se_3$ trilayer vdWHs with (a) A_I stacking for +P case, (b) A_I stacking for –P case, (c) A_{II} stacking for +P case and (d)

A_{II} stacking for –P case.
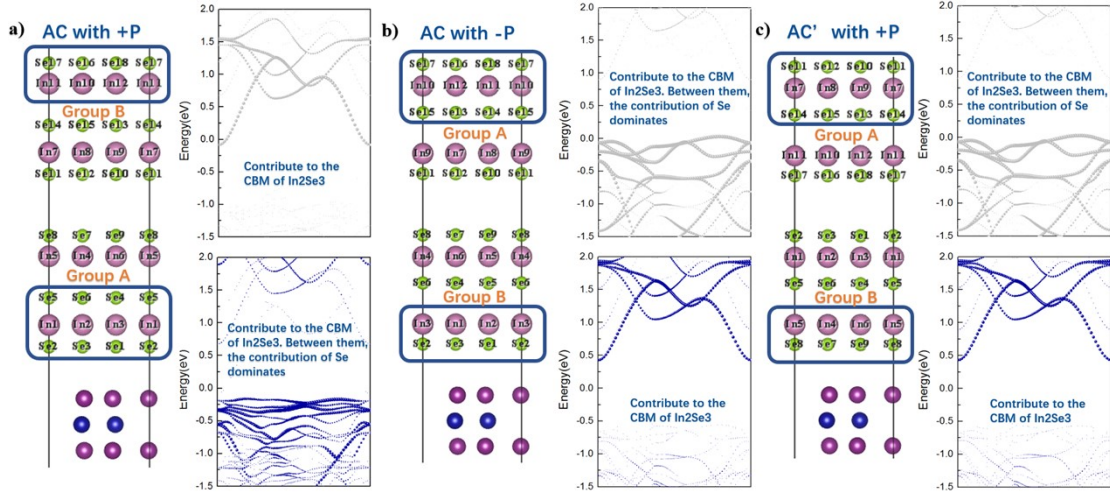
Fig. S9 Contribution of atoms to CBM and VBM for (a) A_I stacking with +P polarization (b) A_I stacking with –P polarization (c) A_{II} stacking with +P polarization.

In order to clarify the internal mechanism of FM effect on FE, the contribution of atoms to CBM and VBM are drawn. From Fig. S9(a-c), we find that the VBM of the In_2Se_3 part is contributed by a set of Se/In/Se atomic layers (marked as group A) with a sandwich structure, of which the main contributions are come from the two Se layers. However, the In_2Se_3 part of the CBM is contributed by a set of two layers of Se/In atomic layers (labeled as group B). Whether the In_2Se_3 band gap is opened or not depends on the B group atoms. For the A_I superposition with –P configuration [Fig. S9(b)], the B group (consisting of 1-3 Se atoms and 1-3 In atoms) is so close to CrI_3 that the band gap of In_2Se_3 is opened under the influence of the magnetic proximity effect. On the contrary, for the A_I stacking with +P polarization [Fig. S9(a)], the B group atoms (consisting of 16-18 Se atoms and 10-12 In atoms) are far away from the influence of FM CrI_3, which tends to maintain the properties of the bilayer In_2Se_3. In order to verify this result, we reversed the polarizations of the two layers of In_2Se_3 separately in A_I stacking with +P case, i.e., the A_{II} superposition with +P configuration [Fig. S9(c)]. And then the new 7-9 Se atoms and 4-6 In atoms

compose a new group B, which is closer to CrI_3. As we conjectured, the band gap of In_2Se_3 is opened. For the case of CrI_3 flipped vertically, the principle is the same to the above. However, owing to the mirror asymmetry, the influence of the flipped CrI_3 on the ferroelectricity is smaller than that before, so that the band gap of In_2Se_3 opened by CrI_3 becomes smaller.
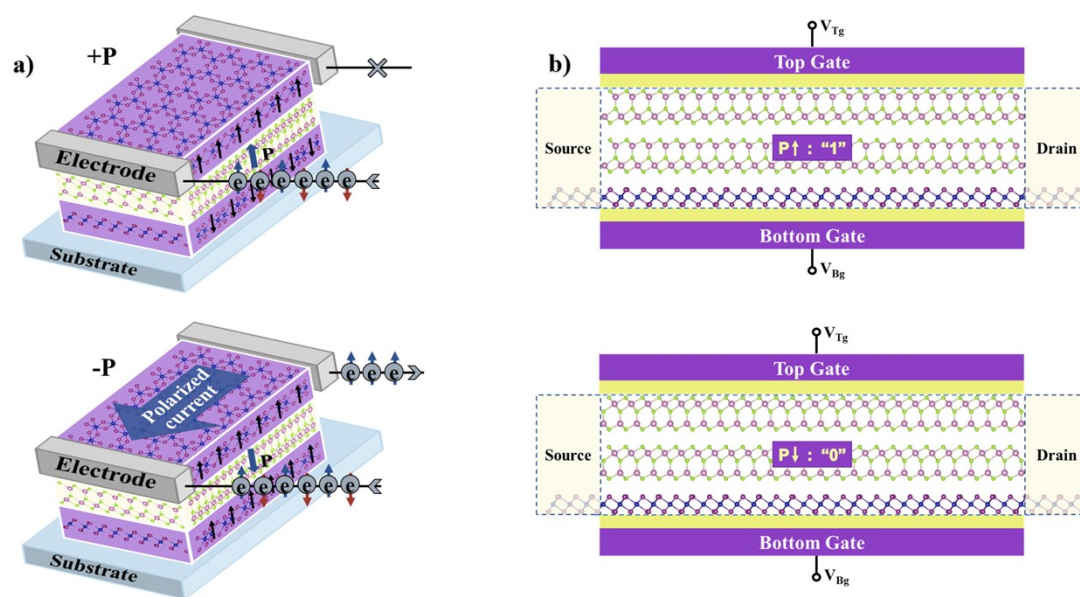
Fig. S10 Two prototypes of spin-field effect transistors (a) atom-thick multiferroic memory devices based on the $CrI_3/In_2Se_3/CrI_3$ vdWH (b) spin switch based on the $CrI_3/2L\text{-}In_2Se_3$ vdWH
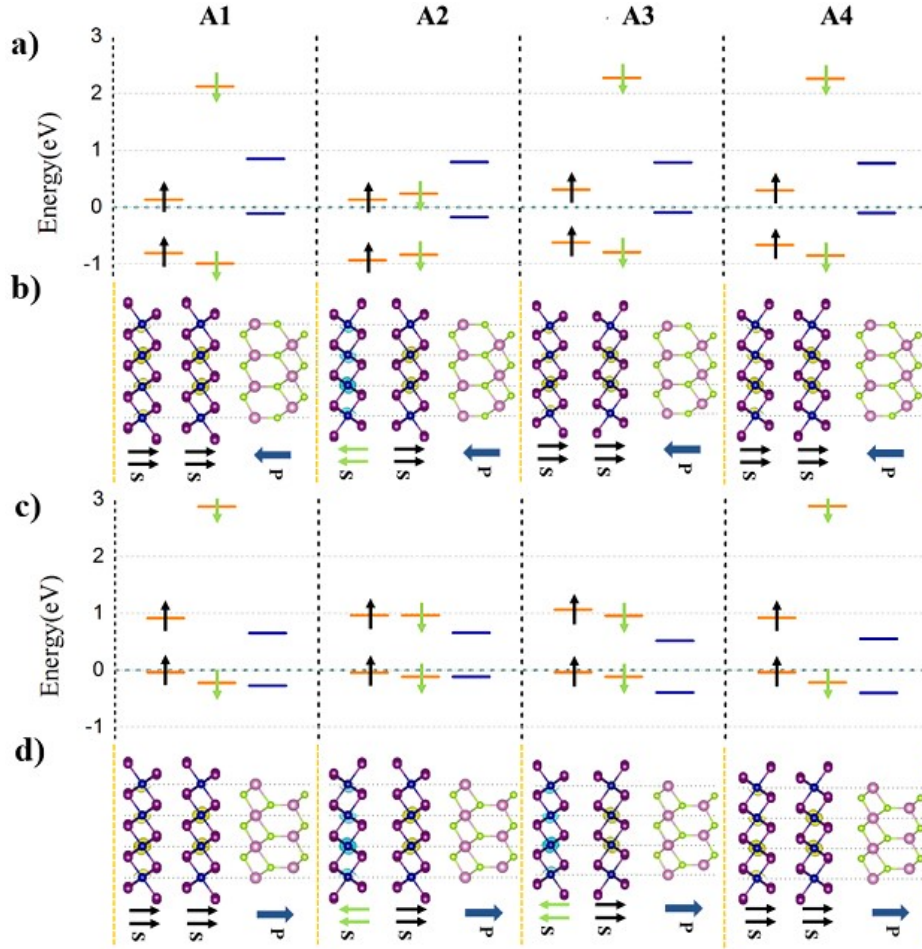
Fig. S11 Band alignments of In$_2$Se$_3$/2L-CrI$_3$ vdWHs with A$_1$, A$_2$, A$_3$ and A$_4$ stackings for (a) +P polarization and (c) –P case, where the orange and dark blue line represent the contribution of CrI$_3$ and In$_2$Se$_3$. And the black and green arrows in (a) and (c) indicate the spin-up channel and the spin-down channel energy level. The A$_1$, A$_2$, A$_3$ and A$_4$ configurations represent the structures without flipping and applying flipping, respectively. The corresponding structure are shown in (b) and (d), where the yellow and blue color around Cr atoms mean the spin-up and spin-down charge distribution. The black and green arrows in (b) and (d) indicate the spin orientation of Cr atoms, and the dark blue arrow represents the direction of FE polarization.

For the vertical In$_2$Se$_3$/2L-CrI$_3$ multiferroic vdWHs, we can construct four typical atomic stackings and place bialyer CrI$_3$ on the side of In$_2$Se$_3$, marked as A$_1$, A$_2$, A$_3$ and A$_4$, shown in Fig. 12(b). For +P case with A$_3$ stacking, the conduction bands near the E$_f$ belong to the spin-down channel associated with the upper CrI$_3$ layer. On the contrary, for the –P case, the

conduction bands near the E_f belong to the spin-up channel associated with the lower CrI$_3$ layer. The result provides the field-dependent spin filtering in which one type of spin current can be switched to another type of spin current through an electric field-induced transition from +P to –P configuration.

Table S1 The lattice constant **a**, interlayer distance **d**, binding energy **E$_b$**, exchange energy **E$_{ex}$** and magnetic ground state **MGS** for CrI$_3$/In$_2$Se$_3$ vdWHs with A, B and C stacking patterns, where +P and –P stand for upward polarization and downward polarization, respectively.

Stackings	P	a(Å)	d	E$_b$(eV/Å^{-2})	Eex(meV)	MGS
A	+P	7.096	3.141	-1.676522	64.029	FM
	-P	7.095	3.171	-1.675411	63.346	FM
B	+P	7.096	3.878	-1.666743	64.116	FM
	-P	7.095	3.889	-1.666096	63.492	FM
C	+P	7.096	3.155	-1.677653	64.285	FM
	-P	7.095	3.179	-1.676339	63.135	FM

To estimate the stability of the 2D multiferroic vdWHs, the binding energy (E$_b$) is calculated by the following expression:

$$E_b = (E_{HS} - E_{In_2Se_3} - E_{CrI_3}) / A$$

where E_{HS}, E_{In2Se3}, E_{CrI3} represent the total energies of the multiferroic vdWHs, isolated CrI$_3$ and In$_2$Se$_3$ monolayer, A is the interfacial area, as shown in Table S1. According to this definition, the more negative the E$_b$ is, the more stable the structure can be in terms of energy. Such negative E$_b$ proves that all stacking configurations are stable. It can be seen from Table S1 that the interlayer distances of +P and –P cases are highly close for the same stacked configuration. Taking the A configuration as example, the interlayer distances along the z direction for CrI$_3$ /(+P)In$_2$Se$_3$ and CrI$_3$ /(-P)In$_2$Se$_3$ vdWHs are 3.14 and 3.17 Å, respectively. Such interlayer distances illustrate the nature of the van der Waals combination between

CrI$_3$ and In$_2$Se$_3$. The interlayer interaction energy difference E_{bis} ($\approx$1.15 meVÅ^{-2}) between the CrI$_3$/(+P)In$_2$Se$_3$ and CrI$_3$/(–P)In$_2$Se$_3$ vdWHs reveals the bistable nature of the heterojunction switch based on FE In$_2$Se$_3$.

Table S2 The average electrons of the Cr-3d orbital in the free-standing monolayer CrI$_3$ and bilayer vdWHs

Stackings	P	t2g		eg		total
		Spin up	Spin down	Spin up	Spin down	
CrI$_3$		2.042500	0.283000	1.714600	0.0858	4.126
A	+P	2.048600	0.273900	1.711600	0.0829	4.117
	–P	2.047500	0.274700	1.711700	0.083	4.1168
B	+P	2.048300	0.273900	1.711400	0.0831	4.1167
	–P	2.046600	0.274600	1.712000	0.0831	4.1163
C	+P	2.046100	0.276000	1.711600	0.0832	4.1169
	–P	2.044500	0.276400	1.711200	0.0844	4.1165

Table S3 The average electrons of the Cr-3d orbital in CrI$_3$/In$_2$Se$_3$/CrI$_3$ vdWHs with A$_1$, A$_2$, A$_3$, and A$_4$ stackings.

P	stacking	atom	t2g		eg		total	MGS
			Spin up	Spin down	Spin up	Spin down		
+P	A$_1$	Cr$_1$	2.0369	0.2817	1.7122	0.0831	4.1139	FM
		Cr$_2$	2.0382	0.2821	1.7121	0.0844	4.1168	
		Cr$_3$	2.0384	0.2796	1.7127	0.0833	4.1140	
		Cr$_4$	2.0372	0.2806	1.7126	0.0823	4.1128	
	A$_2$	Cr$_1$	2.0398	0.2815	1.7126	0.0840	4.1179	FM
		Cr$_2$	2.0391	0.2807	1.7107	0.0844	4.1150	
		Cr$_3$	2.0383	0.2791	1.7120	0.0838	4.1131	
		Cr$_4$	2.0374	0.2804	1.7136	0.0834	4.1149	
	A$_3$	Cr$_1$	2.0382	0.2823	1.7117	0.0836	4.1158	FM
		Cr$_2$	2.0382	0.2808	1.7116	0.0843	4.1149	
		Cr$_3$	2.0369	0.2827	1.7122	0.0840	4.1158	
		Cr$_4$	2.0349	0.2831	1.7130	0.0839	4.1148	
	A$_4$	Cr$_1$	0.2784	2.0392	0.0823	1.7131	4.1129	AFM
		Cr$_2$	0.2790	2.0377	0.0825	1.7125	4.1116	

		Cr$_3$	2.0375	0.2823	1.7110	0.0835	4.1143	
		Cr$_4$	2.0380	0.2818	1.7130	0.0831	4.1160	
−P	A$_1$	Cr$_1$	0.2820	2.0374	0.0835	1.7131	4.1160	AFM
		Cr$_2$	0.2813	2.0378	0.0843	1.7124	4.1159	
		Cr$_3$	2.0395	0.2792	1.7134	0.0824	4.1145	
		Cr$_4$	2.0387	0.2782	1.7131	0.0828	4.1128	
	A$_2$	Cr$_1$	0.2794	2.0391	0.0828	1.7133	4.1146	AFM
		Cr$_2$	0.2798	2.0392	0.0829	1.7130	4.1148	
		Cr$_3$	2.0394	0.2802	1.7124	0.0831	4.1151	
		Cr$_4$	2.0388	0.2804	1.7132	0.0835	4.1160	
	A$_3$	Cr$_1$	2.0356	0.2814	1.7117	0.0839	4.1125	FM
		Cr$_2$	2.0361	0.2807	1.7124	0.0841	4.1133	
		Cr$_3$	2.0372	0.2811	1.7136	0.0834	4.1153	
		Cr$_4$	2.0357	0.2801	1.7133	0.0829	4.1121	
	A$_4$	Cr$_1$	2.0378	0.2807	1.7135	0.0827	4.1147	FM
		Cr$_2$	2.0384	0.2808	1.7121	0.0831	4.1144	
		Cr$_3$	2.0360	0.2806	1.7130	0.0829	4.1124	
		Cr$_4$	2.0377	0.2803	1.7132	0.0838	4.1150	

Table S4. The overview of the applicable devices.

structures	+P	−P	devices
CrI$_3$/In$_2$Se$_3$/CrI$_3$	semiconductor	half-metal	Spin switch
			Atom-thin multiferroic memory device
CrI$_3$/2L-In$_2$Se$_3$	half-metal	semiconductor	Spin switch
			Atom-thin multiferroic memory device
CrI$_3$/2L-CrI$_3$	semiconductor (S↓)	semiconductor (S↑)	Field-dependent spin filtering